



1 **Revisiting the Sunspot Number as EUV proxy for ionospheric F2 critical frequency**

2

3 Bruno S. Zossi^{1,2}, Franco D. Medina^{1,2}, Trinidad Duran^{3,4}, Blas F. de Haro Barbas^{1,2} and Ana G. Elias^{1,2}

4 (1) Laboratorio de Ionosfera, Atmosfera Neutra y Magnetosfera (LIANM), Facultad de Ciencias
5 Exactas y Tecnología (FACET), Universidad Nacional de Tucumán (UNT), Argentina

6 (2) INFINOA, CONICET-UNT, Argentina

7 (3) Departamento de Física, Universidad Nacional del Sur (UNS), Bahía Blanca, 8000, Argentina

8 (4) Instituto de Física del Sur (CONICET-UNS), Bahía Blanca, 8000, Argentina

9

10 **Correspondence to:**

11 Bruno S. Zossi

12 E-mail: bzossi@herrera.unt.edu.ar

13

14 **Abstract:**

15 This study reconsiders the Sunspot Number (S_n) as a solar extreme ultraviolet (EUV) proxy for
16 modeling the ionospheric F2 layer's critical frequency (f_oF_2) over the period 1960-2023. We
17 compare the performance of S_n with F10.7 and F30 solar radio fluxes, focusing on their ability to
18 model the Global Ionospheric index (IG). Our results reveal that while F30 has shown a better
19 correlation in recent solar cycles, the S_n is the most stable and reliable over the entire dataset,
20 obtaining the highest correlation. In addition, if we remove the saturation effects from the
21 considering a maximum value of S_n , the correlation increases, outperforming all other proxies, and
22 predicting correctly the long-term trend estimated by general circulation models.

23 **Plain Language Summary**

24 The Earth's ionosphere, a critical layer for radio communication and GPS signals, is influenced by
25 the Sun's radiation. To understand how the ionosphere changes over time, scientists use
26 measurements of solar activity called proxies. In this study, different proxies are evaluated to find
27 the best one for modeling ionospheric conditions over the last 60 years. Despite being an older
28 measure, we found that the Sunspot Number is the most reliable for long-term studies,
29 outperforming newer proxies in some cases. Our work suggests that relying on newer proxies
30 might lead to inaccurate predictions, especially during periods of low solar activity.

31

32 **Key Points**

- 33 • The Sunspot Number (S_n) outperforms F30 and F10.7 solar proxies in long-term
34 ionospheric datasets, especially before 1980 and during recent solar cycles.
- 35 • Removing the saturation effect from the S_n dataset further enhances its correlation with
36 the Global Ionospheric index (IG), improving long-term trend predictions.



- 37 • The study emphasizes the variable performance of solar proxies over time, with Sn
38 showing the greatest stability for modeling ionospheric conditions across six decades.

39

40 **1. Introduction:**

41 The understanding of atmospheric trends became a critical area of study in the last century.
42 Besides the troposphere, the upper atmosphere is also affected by human activities. Many
43 modern technologies, such as long-distance telecommunications, global positioning systems (GPS),
44 and satellite communications, rely on space and near-Earth physics (Zolesi and Cander, 2014). One
45 important part of the upper atmosphere is the ionosphere, defined as the zone where the
46 presence of free charges is high enough to affect the propagation of electromagnetic waves. Long-
47 term trends in this region arise primarily from the greenhouse effect but are also influenced by
48 long-term solar periodicities and the secular variation of Earth's magnetic field (Lastovicka, 2023).

49 This ionized area is mainly affected by solar extreme ultraviolet radiation (EUV), which is absorbed
50 by the neutral components, heating and ionizing them. To model this atmospheric layer, direct
51 measurements of EUV are needed. However, such data have only been available since the satellite
52 era, therefore, several models were developed using EUV proxies, or, different measurements that
53 are closely linked to the needed variable (Bilitza et al. 2022, Liu et al. 2010). More recent proxies
54 measure solar irradiance at specific wavelengths in satellites, avoiding the interaction with the
55 atmosphere. The most common are magnesium II wing-to-core ratio, helium II, and Lyman-alpha,
56 among others.

57 The ionospheric structure has been measured since the 1930s after the development of the
58 ionosonde. This instrument operates by emitting a vertical electromagnetic wave from the ground
59 and waiting for the reflection of the wave. The internal layers are reached using different
60 frequencies. The ionosphere is mainly studied through ionosonde databases, mainly due to their
61 long period and the reliability of the available data. The main data produced by ionosondes are the
62 critical frequencies and the peak height of each layer.

63 Over the past decades, various solar indices have been employed as proxies for estimating
64 ionospheric parameters. Among these, the Sn has historically been one of the most reliable
65 proxies due to its long record and strong correlation with solar EUV radiation, which directly
66 affects the ionosphere. However, newer solar indices, such as the F10.7 cm solar radio flux
67 (Lastovicka et al. 2006, Mielich and Bremer (2013), Jakowski et al. 2024), and the more recent F30
68 (Lastovicka 2021, Dudok de Wit and Bruinsma 2017, Zossi et al. 2024), as well as MgII (de Haro
69 Barbas et al. 2021), have been introduced as alternatives that may offer better correlations under
70 specific conditions or periods.

71 Recent studies have debated the effectiveness of these proxies, particularly in representing
72 ionospheric trends during periods of low solar activity, such as the deep minima of solar cycles 24
73 and 25. These discussions have highlighted the need for continuous evaluation of solar proxies to
74 ensure accurate long-term trend predictions, which are crucial for both scientific understanding
75 and practical applications in space weather forecasting.

76 In recent years, some articles studied the changes in the relationship between the sunspot
77 number and the solar radio fluxes, identifying a trend associated with the Sun that affects this
78 relationship (Clette 2021, Mursula et al. 2022, 2024). The solar radio fluxes tend to increase



79 compared to the sunspot number, this trend may introduce an error in models, that rely on these
80 indices.

81

82 In this study, we assess the performance of the Sn, F10.7, and F30 as proxies for modeling
83 ionospheric foF2 for the period 1960-2023, particularly focusing on their ability to model the
84 ionospheric index IG, a key indicator of global ionospheric conditions. We examine the stability
85 and correlation of these proxies over different solar cycles and discuss the implications of choosing
86 one proxy over another for long-term ionospheric studies. This procedure results in a better
87 performance of Sn over F10.7 and F30 to reproduce the complete IG dataset, mainly during the
88 complicated solar cycles 20, 23, and 24.

89

90 **2. Data**

91 The foF2 monthly median time series used in this work are from the following 10 stations: Wak-
92 kanai (45.2°N, 141.4°E), Kokubunji (35.7°N, 139.5°E), Okinawa (26.3°N, 127.6°E), Hobart (42.5°S,
93 147.2°E), Canberra (35.2°S, 149.1°E), Townsville (19.2°S, 146.5°E), Sodankyla (67.3°N, 26.3°E),
94 Boulder (40.1°N, 105.2°W), Juliusruh (54.6°N, 13.4°E), and Rome (41.5°N, 12.3°E). The selected
95 stations have long records, covering, in some cases, more than 60 years. Due to the uncertainties
96 and bad reading, some data were discarded. The criteria used to calculate the monthly medians
97 for each hour required at least 15 days available with measurements in every month, and checking
98 outliers in every case. Most of the datasets were extracted from Damboldt and Suessmann data-
99 base (Damboldt and Suessman 2012). The data was updated until 2022 using records from Lowell
100 GIRO Data Center (LGDC) (Reinisch and Galkin 2011). foF2 from the Digital Ionogram Data Base
101 (DIDBase) at LGDC has a frequency of 5 to 15 minutes. To obtain the monthly medians, data with
102 Autoscaling Confidence Score (CS) greater than 60% was first selected, and then the hourly median
103 for each month was estimated. We checked that the last two years available from Damboldt and
104 Suessman database had a reasonable coincidence (within 5%) with the data obtained from GIRO.

105 In this work, the Global Ionospheric index (IG) is used to analyze the solar proxies. IG was originally
106 computed using 13 globally distributed ionosonde stations. The distribution of these stations was
107 a compromise between good global coverage and reliable long-operating-period ionosonde
108 stations. However, due to station closures and data unavailability, the number of stations used in
109 IG has decreased to four (Brown et al., 2018). Therefore, since IG is derived from ionospheric
110 measurements, it captures foF2 variations not driven solely by solar activity, such as those caused
111 by increased greenhouse gases.

112

113 **3. Methodology**

114 In this work, we use linear regressions between the annual averaged IG index, which represents
115 ionospheric foF2, and solar proxies. The linear regression is a simple statistical method that
116 models the relation between two variables using a linear equation,

$$117 \quad y = \alpha_0 + \alpha_1 x \quad (1)$$

118 where α parameters are the regression coefficients, usually estimated using least squares, and \mathbf{x}
119 and \mathbf{y} are the independent and dependent variables, respectively.



120 This regression is widely used for systems highly sensitive to a given variable or parameter. For
121 example, many upper atmosphere parameters, when dealing with annual means, respond to the
122 solar flux almost linearly. We also extend to a second-order regression, which is the same
123 procedure, but adding a squared term of variable x .

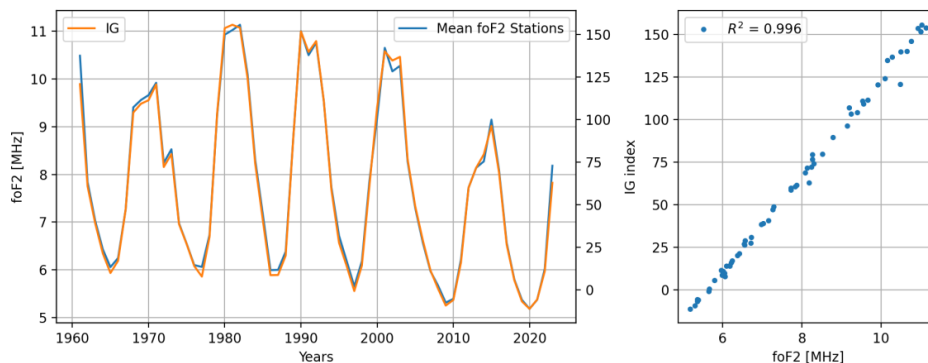
124 To compare the performance of each proxy we use the squared correlation coefficient, R^2 , which
125 provides a measure of the variance of y predicted by the model using the independent variables.

126

127 4. Results and Discussion

128 Using IG index as a global mean ionospheric condition. IG values are scaled to sunspot number, it
129 represents foF2 from different stations around the world. Figure 1 shows the yearly averaged
130 values of foF2 for the stations used in this work and the IG index, the correlation between both is
131 also plotted. With an R^2 of 99.6%, we can say that the IG index is a reliable representation of
132 ionospheric conditions. Therefore, we will use it to compare with the solar EUV proxies.

133



134

135 Figure 1. Yearly noon mean (12 LT) foF2 for the ten stations used in this work (blue), and IG index
136 (orange). The right panel shows the linear correlation between IG and foF2, the explained variance
137 $R^2 = 0.996$.

138

139 The variability of ionospheric foF2, at the interannual scale, is mainly driven by solar activity. For
140 this reason, many (practically any) EUV proxies result in an excellent correlation with annual
141 averaged foF2.

142 As we mentioned, in the last years, many articles have been published trying to find the correct
143 proxy for long-term trend estimation. Among them, the more reliable were always the oldest, the
144 sunspot number, and the solar fluxes at radio wavelengths, having measured datasets of 70 years
145 and more. However, such long datasets for ionospheric conditions are uncommon, just a bunch of
146 measuring stations have reliable data in this period.

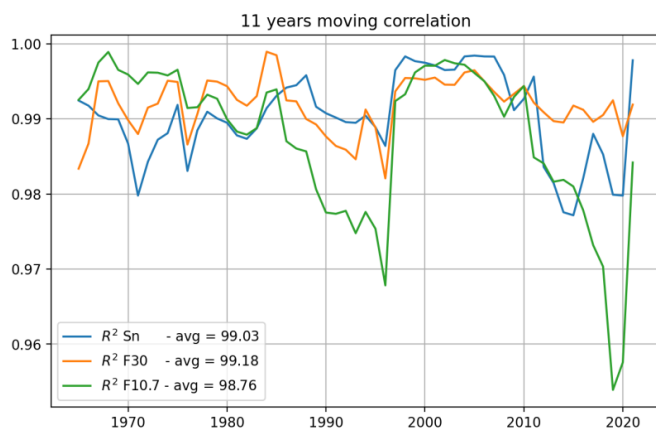
147 Lastovicka (2021) criteria for selecting the best solar proxy include the high correlation, temporal
148 stability, and, the trend estimation having a consistent sign throughout the entire period. Based on
149 these factors, the study concluded that F30 is the most suitable EUV proxy for ionospheric long-



150 term trend estimation. Nevertheless, the trend estimation is compared to general circulation
151 models (Solomon et al. 2018), where the solar activity remains constant while greenhouse gases
152 increase, resulting in a trend of ~ -0.6 %/decade for foF2.

153 As the main issue is to find long ionospheric datasets, in many articles, the trends are often
154 assessed using data up to 2008, avoiding the deep solar minimum, or from 1985 to the present.
155 The important historical issues were the correlation decreasing in some periods and the change in
156 the estimated trend after filtering the solar activity. These problems turn into the necessity of
157 looking for other solar EUV proxies, particularly given the unique characteristics of the last solar
158 cycles 24 and 25, which featured two deep minima with prolonged periods of zero sunspot
159 numbers. During these deep minima, the ionospheric foF2 drops below historical minimum values,
160 this fact can be easily noted since the IG index takes the most quantity of negative values in the
161 last two cycles.

162 The stability of the correlation between proxies and data results in a slight average correlation of
163 F30 over Sn and F10.7. This can be seen in Figure 2, where an 11-year centered moving correlation
164 was calculated between IG and the three proxies. F10.7 shows two periods of lower correlation,
165 this is a key reason for the need to use another proxy. On average, F30 has a higher correlation
166 using this comparative analysis, especially in the last cycle, where correlations for the other
167 proxies decrease. Sn has a step down in this last cycle but is the best from 1990 to 2008
168 approximately, where solar fluxes have a noticeable correlation decrease.



169
170 Figure 2. 11-year moving squared linear correlation between IG and solar EUV proxies: Sn (blue),
171 F30 (orange), and F10.7 (green).

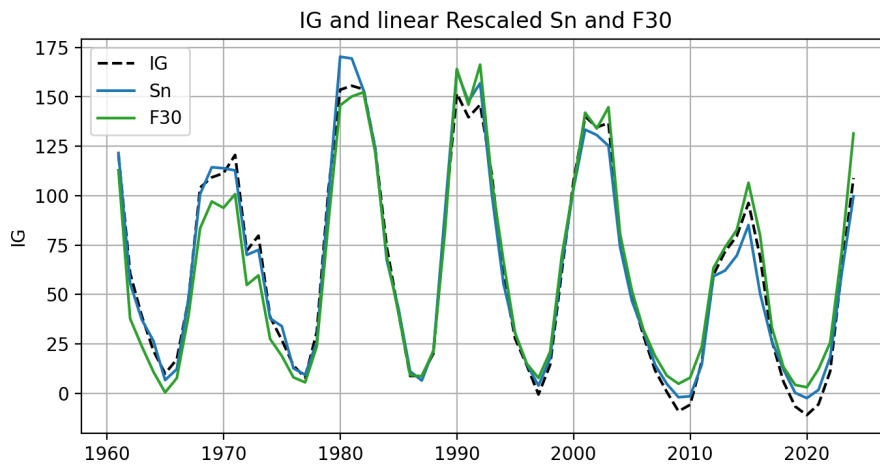
172

173 The linear correlation analysis indicates that Sn and F30 are better reproducing the variability of
174 foF2, through the IG index. Figure 3 shows the IG values modeled linearly using both proxies along
175 with the original dataset. This figure helps to contextualize the moving correlation seen in Figure 2.
176 In all maximums after 1980, F30 is closer to IG values, however, in the complete previous solar
177 cycle; Sn models better the ionospheric index. On the other hand, during minimum solar periods,
178 Sn outperforms F30, even during the last two deep minimum cycles. Taking into account that Sn



179 has a minimum possible value of zero, is expected to fail to reproduce these last two cycles,
180 however, F30 does not reproduce the IG index decrease.

181



182

183 Figure 3. Linear modeling of the ionospheric IG index using F30 (green) and Sn (blue), with the
184 observed IG index (black dashed line).

185

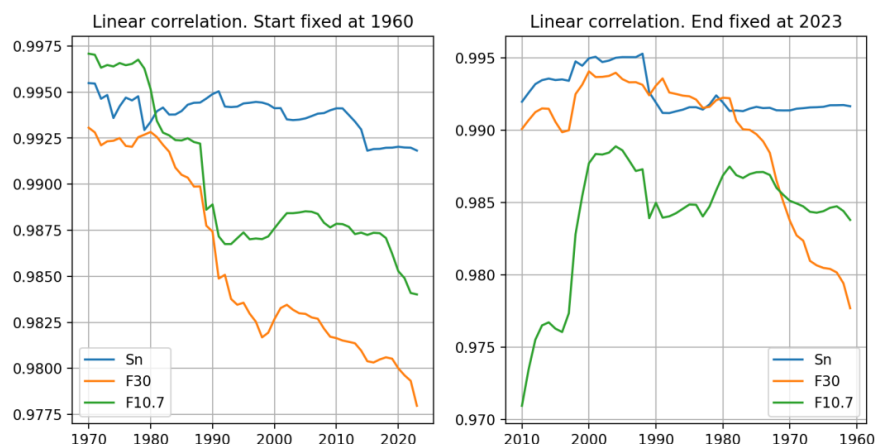
186 There is a clear trend between Sn and F30, note in Figure 3 how F30 (green line) is under the Sn
187 (blue line) up to ~1990, where two lines cross, and after this time, F30 models higher values of IG
188 at almost every point. This behavior is closely linked to the analysis made by Mursula et al. (2024);
189 they compare the solar flux indices with the sunspot number, recognizing this increasing trend.

190 At this point, an important problem arises, if solar fluxes increase compared to IG, which
191 represents ionospheric foF2 level, we can anticipate a decreasing trend in the residuals if we
192 subtract IG modeled with F30 from the original data. Perhaps, looking for a proxy with a
193 decreasing trend led us to a mistake with F30, mainly, taking into account that F30 do not obtain
194 the highest correlation before ~1980.

195 This can be noted in Figure 4, where we perform an ending point moving correlation, fixing the
196 first year in 1960, changing the last year, and calculating the linear correlation of IG and the three
197 proxies. Additionally, the same analysis is performed in reverse, fixing the final year at 2023,
198 changing the first year, and estimating the linear correlation. In Figure 4, the superior performance
199 of Sn to predict IG is clear, the left panel shows that starting the analysis in 1960, Sn is the best in
200 almost the complete period, except for F10.7 at the beginning. On the other hand, the right panel
201 explains why F30 is sometimes considered the best, fixing the last year and adding years backward
202 in time, can be noted that, if the correlation analysis begins in the period 1980-1990, F30 is is the
203 the best, but looking the complete panel, is clear that is just for that period. This is clearer comparing
204 with Figure 3, where we noted that F30 fails to model the beginning and the end of the IG dataset.
205 Moreover, Sn has a clear higher stability in this kind of analysis, therefore, the question is: why are
206 we discarding Sn as a solar EUV proxy?



207 Note that the analysis of Figure 4 is completely different from the result of Figure 2, due to the
208 variation in the initial and ending years, the result of the best correlation using F30 can be
209 obtained reducing the period used in the correlation. This discrepancy is associated with the
210 inclusion, or not, of solar cycle 20 (1964-1976), where F30 does not represent properly the IG
211 index variability.



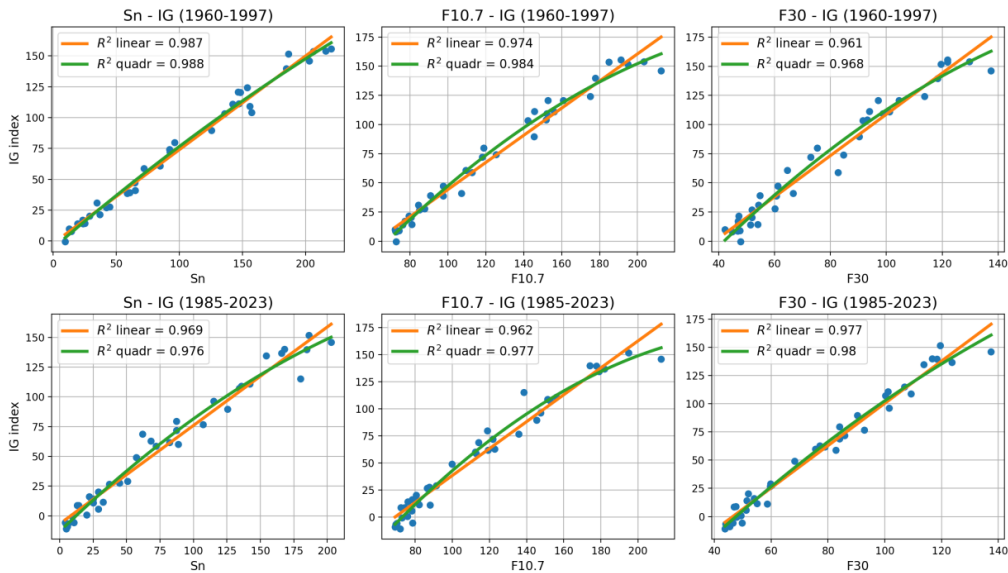
212

213 Figure 4. Squared linear correlation between IG and Sn, F30 and F10.7 with moving end year (left),
214 and inverse, moving start year (right).

215

216 An important ionospheric feature is the saturation (Balan et al., 1994; Liu et al., 2003). During the
217 daytime, there is a maximum possible value of foF2, even if solar flux continues increasing. This
218 problem is more evident at shorter time scales. Many authors deal with this by performing a
219 quadratic and even cubic regression between proxies and foF2 (Liu et al., 2006; Ma et al., 2009;
220 Danilov and Berbeneva, 2023). However, this effect is not that clear when analyzing annual means.
221 Figure 5 shows the linear and quadratic regression between proxies and IG separately for periods
222 1960-1997, and 1985-2023, to have the same number of years in each regression. Again, we can
223 mention the higher performance of Sn in the first cycles, and F10.7 is the second-best proxy. In
224 contrast, F30 obtains a higher correlation in the second period. There is a weak improvement
225 using quadratic regression at the annual scale, this can be noticed in each panel. The F10.7 exhibits
226 a more significant increase in the correlation.

227

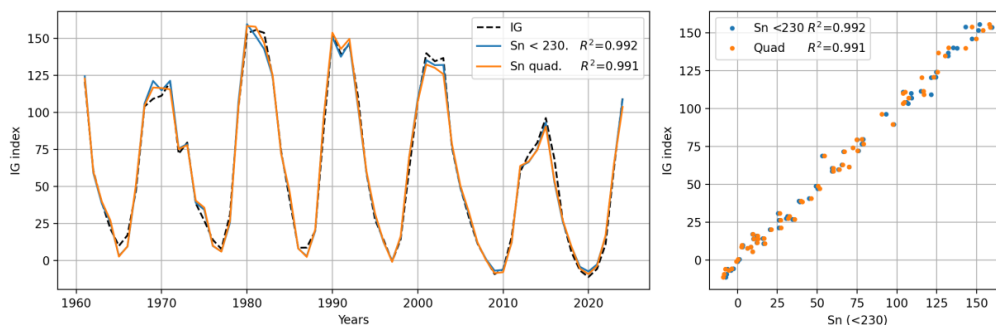


228

229 Figure 5. Linear and quadratic regression between proxies and IG separately for periods 1960-1997
 230 (top panels), and 1985-2023 (bottom panels).

231 Is then the sunspot number the best EUV proxy to model foF2? The evidence up to this point
 232 suggests that is more stable considering longer datasets. The saturation effect could be affecting
 233 the correlation, therefore, subtracting from the daily dataset the Sn higher than 230 (~5% of data)
 234 and calculating the annual mean we obtain an excellent improvement in the linear correlation
 235 between Sn and IG. This method can be also used with F30 and F10.7, but the improvement is not
 236 as good as with the sunspot number (see Table 1). In addition, we model the annual IG using a
 237 quadratic regression; both results can be seen in Figure 6. Since Sn is the only proxy that shows
 238 the down step between cycle 23 and 24 minimums, like IG and most ionospheric stations, it
 239 obtains the highest correlation using the complete period.

240



241

242 Figure 6. IG index (black dashed) and IG index modeled using quadratic regression (orange) and Sn
 243 de-saturated (<230, blue). The right panel shows IG vs IG modeled.



244

245 The correlation using a de-saturated Sn and quadratic regression shows a significant improvement
246 over the original dataset, compared to Sn in Figure 3. The maximums of all cycles after 1970 are
247 close to IG values. Moreover, the last two minimums are much better represented using the
248 quadratic regression and de-saturating the Sn dataset. The squared correlations between indices
249 and stations using quadratic regression can be seen in Table 1, compared to linear and de-
250 saturated Sn. The Table shows that quadratic regression using Sn is, on average, the most effective
251 to predict the ionospheric foF2, followed by Sn de-saturated and quadratic F10.7.

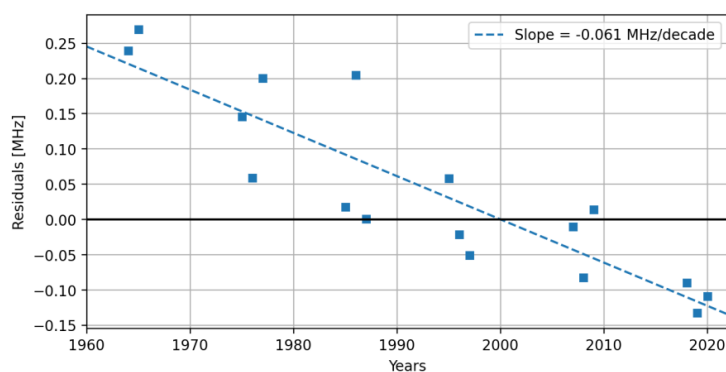
252

253 Table 1. Squared correlation (R^2) between stations and indices using a quadratic regression over
254 the complete period (1960-2023), compared with linear and de-saturated Sn.

	Sn linear	F30 quad	F10.7 quad	Sn quad	Sn (<230)
Okinawa	0.917	0.859	0.940	0.944	0.939
Wakkanai	0.967	0.968	0.966	0.970	0.968
Kokubunji	0.981	0.979	0.984	0.989	0.988
Townsville	0.947	0.921	0.968	0.972	0.967
Canberra	0.980	0.972	0.983	0.988	0.989
Hobart	0.974	0.975	0.976	0.980	0.980
Juliusruh	0.983	0.981	0.978	0.984	0.981
Rome	0.970	0.971	0.976	0.979	0.978
Boulder	0.953	0.950	0.957	0.962	0.965
Sodankyla	0.911	0.900	0.901	0.911	0.907
Average	0.958	0.947	0.963	0.968	0.966

255

256 The only remaining task is the estimation of the long-term trend using a highly reliable proxy.
257 From Figure 6, we can expect a nearly zero trend for the complete period. This is confirmed by
258 filtering the solar activity from the IG dataset using de-saturated Sn and calculating the residuals,
259 which yield a trend of -0.008 %/decade. However, if we take a close look at the minimum's solar
260 times in Figure 6, a clear trend can be noted: IG is higher than Sn in 1965 but lower in 2020.
261 Considering that the CO2 cooling effect over the thermosphere is more pronounced during
262 minimum solar conditions (Emmert et al. 2008, Brown et al. 2024), we could assume a more
263 noticeable effect over the ionospheric parameters as well during lower solar conditions. The
264 theoretical trend estimated using a general circulation model (WACCM-X) is -0.6 %/decade for
265 foF2 (Solomon et al. 2018). Therefore, by focusing on the minimum solar years (1963-1965, 1975-
266 1977, 1985-1987, 1995-1997, 2007-2009, 2018-2020), the trend results in -0.79 %/decade, really
267 close to the theoretical value. The residuals from this procedure are shown in Figure 7, where a
268 clear and constant trend is noticed.



269

270 Figure 7. Residuals for solar cycle minimums years using Sn de-saturated.

271

272 5. Conclusions

273 In this work, we found that the sunspot number is the most reliable solar EUV proxy for predicting
274 ionospheric index IG over the period 1960-2023. This index is a good indicator of the global
275 ionospheric foF2, as is shown in Figure 1, and supporting by the R^2 value.

276 While many recent articles claim F30 as the superior solar EUV proxy, it fails at representing the
277 step down during the last two solar minimums—a decline that is evident in the Sn dataset. Some
278 of these studies analyze shorter periods in order to use more stations. In Figure 2, we show that
279 F30 is the proxy with better stability to represent each cycle separately. However, analyzing the
280 period 1960-2023, Sn outperforms the F30 correlation, as shown in Figure 3.

281 The main issue with F10.7 and F30 is the last two solar cycle minimums, where the ionospheric
282 foF2 decreases more than expected, and a linear model cannot reproduce this decrease using the
283 solar radio fluxes. The sunspot number, on the other hand, effectively handles this issue. When
284 applying a quadratic regression, or neglecting saturation effects from the daily database, Sn
285 obtains the highest correlation, reproducing reliably the last two cycles.

286 The only problem with this methodology is that if we calculate the long-term trend filtering the
287 solar activity, we do not obtain the trend predicted by the global circulation models. Nevertheless,
288 as we point out in Figure 6, minimum solar activity periods have a noticeable trend that results to
289 be in good agreement with the theoretical trend.

290

291 Competing interests

292 At least one of the co-authors is a member of the editorial board of *Annales Geophysicae*.

293

294 Acknowledgment

295 B.S. Zossi, F.D. Medina, and A.G. Elias acknowledge research projects PIP 2957 and PIUNT E756. T.
296 Duran acknowledges research projects PICT 2019-03491 and PGI 24/F083.



297 **Open Research**

298 All data used in this work are in public domain. For ionospheric foF2 (1) National Institute of
299 Information and Communications Technology, NICT
300 (https://wdc.nict.go.jp/IONO/HP2009/ISDJ/manual_txt-E.html). (2) The Australian Bureau of
301 Meteorology (<https://downloads.sws.bom.gov.au/wdc/iondata/au/>). (3) The Lowell GIRO Data
302 Center (<https://giro.uml.edu/didbase/scaled.php>). F10.7 at [https://spaceweather.gc.ca/forecast-
303 prevision/solar-solaire/solarflux/sx-en.php](https://spaceweather.gc.ca/forecast-
303 prevision/solar-solaire/solarflux/sx-en.php). Sn from the revised Sn database obtained from SILSO
304 (Sunspot Index and Long-term Solar Observations), Royal Observatory of Belgium, at
305 <https://www.sidc.be/SILSO/datafiles>, F30 from the National Astronomical Observatory of Japan at
306 http://solar.nro.nao.ac.jp/norp/html/daily_flux.html.

307

308 **References**

309 Balan, N., Bailey, G. J., & Moffett, R. J. (1994). Modeling studies of ionospheric variations
310 during an intense solar cycle. *Journal of Geophysical Research: Space Physics*,
311 99(A9), 17467–17475. <https://doi.org/10.1029/94JA01262>

312 Bilitza, D., Pezzopane, M., Truhlik, V., Altadill, D., Reinisch, B. W., & Pignalberi, A.
313 (2022). The International Reference Ionosphere Model: A Review and Description of
314 an Ionospheric Benchmark. *Reviews of Geophysics*, 60(4), e2022RG000792.
315 <https://doi.org/10.1029/2022RG000792>

316 Brown, M. K., Lewis, H. G., Kavanagh, A. J., Cnossen, I., & Elvidge, S. (2024). Future
317 Climate Change in the Thermosphere Under Varying Solar Activity Conditions. *Jour-
318 nal of Geophysical Research: Space Physics*, 129(9), e2024JA032659.
319 <https://doi.org/10.1029/2024JA032659>

320 Clette, F. (2021). Is the F10.7cm – Sunspot Number relation linear and stable? *Journal of
321 Space Weather and Space Climate*, 11, 2. <https://doi.org/10.1051/SWSC/2020071>

322 Damboldt T, Suessmann P (2012). Consolidated Database of Worldwide Measured Month-
323 ly Medians of Ionospheric Characteristics foF2 and M(3000)F2. INAG (Ionosonde
324 Network Advisory Group) Bulletin 73
325 [https://www.ursi.org/files/CommissionWebsites/INAG/web-
326 73/2012/damboldt_consolidated_database.pdf](https://www.ursi.org/files/CommissionWebsites/INAG/web-
326 73/2012/damboldt_consolidated_database.pdf)

327 Danilov, A. D., Berbeneva, N. A., & Konstantinova, A. V. (2024). Trends in the F2-layer
328 parameters to 2023. *Advances in Space Research*, 73(12), 6054–6065.
329 <https://doi.org/10.1016/J.ASR.2024.03.036>

330 Danilov, A. and Berbeneva, N. (2023). Statistical analysis of the critical frequency foF2
331 dependence on various solar activity indices, *Advances in Space Research*.



- 332 de Haro Barbás, B. F., Elias, A. G., Venchiarutti, J. V., Fagre, M., Zossi, B. S., Tan Jun, G.,
333 & Medina, F. D. (2021). MgII as a Solar Proxy to Filter F2-Region Ionospheric Pa-
334 rameters. *Pure and Applied Geophysics*, 178(11), 4605–4618.
335 <https://doi.org/10.1007/S00024-021-02884-Y>
- 336 Dudok De Wit, T., & Bruinsma, S. (2017). The 30 cm radio flux as a solar proxy for ther-
337 mosphere density modelling. *Journal of Space Weather and Space Climate*, 7, A9.
338 <https://doi.org/10.1051/SWSC/2017008>
- 339 Emmert, J. T., Picone, J. M., & Meier, R. R. (2008). Thermospheric global average density
340 trends, 1967–2007, derived from orbits of 5000 near-Earth objects. *Geophysical Re-*
341 *search Letters*, 35(5), 5101. <https://doi.org/10.1029/2007GL032809>
- 342 Jakowski, N., Hoque, M. M., & Mielich, J. (2024). Long-term relationships of ionospheric
343 electron density with solar activity. *Journal of Space Weather and Space Climate*, 14,
344 24. <https://doi.org/10.1051/SWSC/2024023>
- 345 Laštovička, J., Mikhailov, A. V., Ulich, T., Bremer, J., Elias, A. G., Ortiz de Adler, N., Ja-
346 ra, V., Abarca del Rio, R., Foppiano, A. J., Ovalle, E., & Danilov, A. D. (2006). Long-
347 term trends in foF2: A comparison of various methods. *Journal of Atmospheric and*
348 *Solar-Terrestrial Physics*, 68(17), 1854–1870.
349 <https://doi.org/10.1016/J.JASTP.2006.02.009>
- 350 Laštovička, J. (2021). The best solar activity proxy for long-term ionospheric investiga-
351 tions. *Advances in Space Research*, 68(6), 2354–2360.
352 <https://doi.org/10.1016/J.ASR.2021.06.032>
- 353 Laštovička, J. (2023). Progress in investigating long-term trends in the mesosphere, ther-
354 mosphere, and ionosphere. *Atmospheric Chemistry and Physics*, 23(10), 5783–5800.
355 <https://doi.org/10.5194/ACP-23-5783-2023>
- 356 Liu, H. L., Foster, B. T., Hagan, M. E., McInerney, J. M., Maute, A., Qian, L., Richmond,
357 A. D., Roble, R. G., Solomon, S. C., Garcia, R. R., Kinnison, D., Marsh, D. R., Smith,
358 A. K., Richter, J., Sassi, F., & Oberheide, J. (2010). Thermosphere extension of the
359 Whole Atmosphere Community Climate Model. *Journal of Geophysical Research:*
360 *Space Physics*, 115(A12), 12302. <https://doi.org/10.1029/2010JA015586>
- 361 Liu, L., Wan, W., Ning, B., Pirog, O., and Kurkin, V. (2006). Solar activity variations of
362 the ionospheric peak electron density, *Journal of Geophysical Research: Space Phys-*
363 *ics*, 111.
- 364 Liu, J. Y., Chen, V. I., & Lin, J. S. (2003). Statistical investigation of the saturation effect
365 in the ionospheric foF2 versus sunspot, solar radio noise, and solar EUV radiation.
366 *Journal of Geophysical Research: Space Physics*, 108(A2), 1067.
367 <https://doi.org/10.1029/2001JA007543>



- 368 Ma, R., Xu, J., Wang, W., & Yuan, W. (2009). Seasonal and latitudinal differences of the
369 saturation effect between ionospheric NmF2 and solar activity indices. *Journal of Ge-*
370 *ophysical Research: Space Physics*, 114(A10), 10303.
371 <https://doi.org/10.1029/2009JA014353>
- 372 Mielich, J., & Bremer, J. (2013). Long-term trends in the ionospheric F2 region with differ-
373 ent solar activity indices. *Annales Geophysicae*, 31(2), 291–303.
374 <https://doi.org/10.5194/ANGE0-31-291-2013>
- 375 Mursula, K., Qvick, T., Holappa, L., & Asikainen, T. (2022). Magnetic Storms During the
376 Space Age: Occurrence and Relation to Varying Solar Activity. *Journal of Geophysi-*
377 *cal Research: Space Physics*, 127(12), e2022JA030830.
378 <https://doi.org/10.1029/2022JA030830>
- 379 Mursula, K., Pevtsov, A. A., Asikainen, T., Tähtinen, I., & Yeates, A. R. (2024). Transition
380 to a weaker Sun: Changes in the solar atmosphere during the decay of the Modern
381 Maximum. *Astronomy & Astrophysics*, 685, A170. [https://doi.org/10.1051/0004-](https://doi.org/10.1051/0004-6361/202449231)
382 [6361/202449231](https://doi.org/10.1051/0004-6361/202449231)
- 383 Reinisch, B. W., Galkin, I. A., (2011). Global Ionospheric Radio Observatory (GIRO). *Earth*
384 *Planet Sp* 63, 377–381. <https://doi.org/10.5047/eps.2011.03.001>
- 385 Solomon, S. C., Liu, H. L., Marsh, D. R., McInerney, J. M., Qian, L., & Vitt, F. M. (2018).
386 Whole Atmosphere Simulation of Anthropogenic Climate Change. *Geophysical Re-*
387 *search Letters*, 45(3), 1567–1576. <https://doi.org/10.1002/2017GL076950>
- 388 Zolesi, B., & Cander, L. R. (2014). Ionospheric prediction and forecasting. *Ionospheric*
389 *Prediction and Forecasting*, 1–240. <https://doi.org/10.1007/978-3-642-38430-1>
- 390 Zossi, B. S., Medina, F. D., Duran, T., & Elias, A. G. (2024). Selecting the best solar EUV
391 proxy for long-term timescale applications. *Advances in Space Research*.
392 <https://doi.org/10.1016/J.ASR.2024.07.023>
- 393